International Journal of Structural In

An Artificial Neural Network Model for Determining Stress Concentration Factors for Fatigue Design of Tubular T-joint Under Compressive Loads.

Journal:	*International Journal of Structural Integrity*
Manuscript ID	IJSI-02-2024-0034.R2
Manuscript Type:	Research Paper
Keywords:	Artificial neural network, stress concentration factor, fatigue design, finite element analysis, T-joint

An Artificial Neural Network Model for Determining Stress Concentration Factors for Fatigue Design of Tubular T-joint Under Compressive Loads.

Abstract:

Purpose – The stress concentration factor (SCF) is commonly utilized to assess the fatigue life of a tubular T-joint in offshore structures. Parametric equations derived from experimental testing and finite element analysis (FEA) are utilized to estimate the SCF efficiently. The mathematical equations provide the SCF at the crown and saddle of tubular T-joints for various load scenarios. Offshore structures are subjected to a wide range of stresses from all directions, and the hotspot stress might occur anywhere along the brace. It is critical to incorporate stress distribution since using the single-point SCF equation can lead to inaccurate hotspot stress and fatigue life estimates. As far as we know, there are no equations available to determine the SCF around the axis of the brace.

Design/methodology/approach –A mathematical model based on the training weights and biases of artificial neural networks (ANNs) is presented to predict SCF. 625 FEA simulations were conducted to obtain SCF data to train the ANN.

Findings – Using real data, this ANN was used to create mathematical formulas for determining the SCF. The equations can calculate the SCF with a percentage error of less than 6%.

Originality/value – Precisely determining the SCF for the fatigue life of offshore structures reduces the potential hazards associated with fatigue failure, thereby guaranteeing their longevity and reliability. The present study offers a systematic approach for using FEA and ANN to calculate the stress distribution along the weld toe and the SCF in T-joints since ANNs are better at approximating complex phenomena than standard data fitting techniques. Once a database of parametric equations is available, it can be used to rapidly approximate the SCF, unlike experimentation, which is costly and FEA, which is time consuming.

Keywords: T-joint, Artificial neural network, stress concentration factor, fatigue design, finite element analysis

Nomenclature: D = chord diameter; d = brace diameter; T = chord thickness; t = brace thickness; θ = angle between the brace and the chord; L = chord length; ℓ =brace length; β = ratio of the diameter of brace and chord; γ = ratio of chord's diameter and twice chord's thickness; τ= ratio of brace thickness to chord thickness; α = ratio of twice the length of the chord to the diameter of the chord; α_b = ratio of twice the length of brace to the diameter of the brace; r= brace radius; t= brace thickness; SCF = stress concentration factors; ANN= Artificial neural network; FEA= Finite element analysis; DOE= Design of experiments; R^2 = Coefficient of determination; IPB= In-Plane bending loads, OPB= Out-of-Plane bending loads; i_{max} = maximum of original input data; i_{min} = minimum of original input data; o_{max} = maximum of SCF data used for training; o_{min} = minimum of SCF data used for training; F=force applied on the top of the brace; AWS = The American welding society; IIW = international institute of welding; API= American Petroleum Institute; DNN= Deep learning neural network; GA= genetic algorithm; GBDT= Gradient Boosting Decision Trees; $\sigma_{nominal\ stress}$ = Nominal brace stress applied on brace; $\sigma_{hotspot\ stress}$ = Maximum stress along the weld toe; FFNN = feed-forward neural network design; DNV= Det Norske Veritas; UEG = Underwater engineering group; HSS= Hotspot stress; CHS= Circular hollow sections; RHS= Rectangular hollow sections; SHS= Square hollow sections; N= Fatigue load cycles; σ_1 , σ_2 = Stresses at Extrapolation points; Bx; bias value; A(x)= activation function; hnx= Neurons in the hidden layer ipx=input parameters; WWx= ANN weights

1. INTRODUCTION

Offshore structures experience cyclic wave loading, and determining the fatigue life of welded tubular connections is crucial for ensuring the structural integrity and safe operation of these structures [1]. The SCF is the ratio between the hot-spot stress (HSS) and the nominal brace load and is crucial in assessing the fatigue life of offshore joints [2] along with the S-N curve and HSS [3]–[5]. The SCF is dependent upon various factors, including joint geometry, loading conditions, weld size and type, and proximity to the weld. In the last five decades, extensive research has been dedicated to the establishment of precise parametric equations for stress concentration factors (SCFs) [6]–[12]. Precisely determining the SCF for the fatigue life of offshore structures reduces the potential hazards associated with fatigue failure, thereby guaranteeing their longevity and reliability. The HSS is the maximum stress around the weld toe, and it is the point where the crack is most likely to initiate [1]. The calculation of HSS can be readily determined by utilizing the nominal stress and the SCF. Once HSS is achieved, the number of load cycles (N) can be calculated using the S-N curves provided in the design codes [13].

The fatigue performance of tubular joints is conventionally evaluated using experimental testing and FEA. Expensive experimental testing is usually done to verify the numerical model. Further analysis is conducted utilizing the numerical model. Alternatively, empirical equations derived from FEA are additionally used. The quality of FEA has improved due to the development of advanced computational hardware and software.

Additionally, there have been enhancements in the modeling of mathematical equations. Nevertheless, the integration of complex nonlinear patterns into the SCF equations has not been extensively implemented. While equations derived from regression of FEA datasets based on statistical methods are simple, the resulting SCF is inaccurate. ANN is an efficient tool for modeling complicated real-world phenomena. ANN surpasses statistical methods that depend on simpler assumptions and are capable of accurately estimating the SCF in offshore joints.

Jacket-type offshore platforms are formed with circular hollow sections (CHS) tubular segments. Branching components, known as braces, are welded to the main structure or chord, creating tubular joints. The joints play an important role in the structural integrity of the structures [14]. The T-joint is among the most used tubular joints. As shown in Figure 1, the circular brace is welded at 90° to the main chord. The definitions of parameters are given in Equations 1-5 in Figure 1.

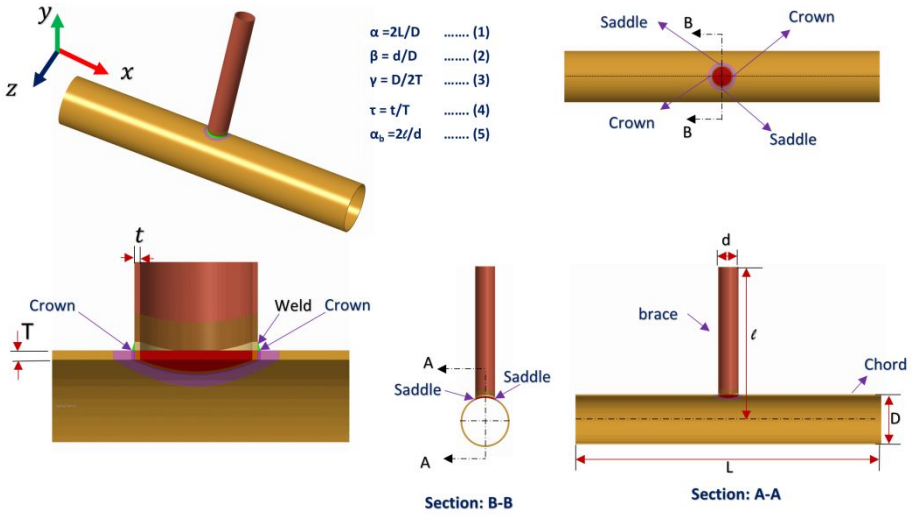

Figure 1: A typical Tubular T joint.

Other hollow sections are rectangular hollow sections (RHS), square hollow sections (SHS), and hybrid CHS-SHS, CHS-RHS and SHS-RHS hollow sections [15]–[19]. Circular hollow sections are commonly utilized in offshore structures [20] for their high bending strength, high strength-to-weight ratio, non-directional buckling, and low wave resistance [21].

Because of the multidirectional character of sea states, offshore structures are subjected to multiaxial loading, which is a combination of axial and bending moments. As a result, the HSS can be situated anywhere around the intersection [22]. Following an examination of the impacts of member and load interaction, Gulati et al. [23] proposed that the HSS be calculated by superimposing the stress distributions of all uni-axis load modes. The UEG [11] recommends this approach since it is the most precise and comprehensive method for determining the stress range at places around the outer edge of the intersection. However, this is not typically used for T-joints due to the limitations of existing parametric equations. These models can only determine the SCFs at the crown and saddle, while the maximum SCF may occur around the weld toe between the crown and saddle positions, which may result in an imprecise estimation of the maximum SCF and the corresponding fatigue life [24].

Over the past 35 years, several parametric formulas have been developed to estimate SCFs for tubular joints [6]–[12]. The UK Health and Safety Executive [8] report, published by Lloyd's Register, conducted a thorough evaluation of the existing parametric equations used for basic tubular joints. These new formulas were developed through experimental analysis of specimens with tubular joints made of acrylic and steel. The Lloyd's Register (LR) equations [8] were obtained by fitting the extracted SCF database, minimizing the discrepancy between the recorded and estimated SCF values at the saddle and the crown positions [25].

Smedley and Fisher [6] formulated parametric equations for single-plane joints (KT, Y, X, T, and K). However, these equations cannot determine SCF along the weld line [25]. The Hellier, Connolly, and Dover (HCD) equations [7] were developed largely to enhance the accuracy of predicting the remaining lifespan of a joint using fracture mechanics principles. However, they are not capable of capturing the impacts of every geometric parameter and may not yield results that are adequately precise for individual joints [22], as the equations were developed from a restricted sampling.

Kauang et al. [9] derived parametric equations for the stress concentration factors of KT, K, T, and Y joints using a finite element program. The Kuang equations were obtained using the statistical evaluation of the data obtained from

the examination of FE joints. The precise position of the hot-spot stress surrounding the weld is not known; instead, it is broadly determined as chord-side or brace-side. The equations fail to account for the impact of the chord length on the saddle caused by the constraints at the ends of the chord. Therefore, it is likely that the SCFs for longer chord lengths (α) are underestimated as the set of finite elements (FE) joints utilized by Kuang consisted predominantly of shorter chord lengths [8]. The Wordsworth/Smedley (W/S) equations were generated based on acrylic model test results for tubular joints modeled without a weld fillet. The parametric equations proposed by Wordsworth [10] specifically address the saddle and crown positions. However, it is not known if intermediate locations were considered, especially in cases where the hot-spot stress is near the saddle and crown [8].

The UEG [11] equations are derived from the W/S and Wordsworth equations, with a modification factor for configurations with high γ (γ >20) and β (β>0.6) numbers. However, Vinas-Pich [22] determined that the UEG stress distribution equations [11] are not sufficiently accurate across the whole brace-chord junction. Efthymiou [12] presented an extensive set of mathematical equations that describe KT, X, T, Y and K joint designs. These equations calculate the SCF at the crown and saddle positions. They provide the closest approximation to the average fit, resulting in frequent underpredictions [8]. The equations developed by Efthymiou [12] are currently utilized in ISO-19902 [26], as well as in the recommendations provided by DNV [27] and the American Petroleum Institute API [28]. Linear regression equations typically provide the SCF values at the saddle and crown positions. Still, they may underestimate SCF if it is situated between these positions.

Recent studies [29]–[32] have employed several machine learning techniques, including deep learning neural networks [29], deep neural networks optimized with genetic algorithms [30] and particle swarm algorithms [31], as well as ANN with Gradient Boosting Decision Trees (GBDT) [32]. The advantages of ANN lie in its ability to perform universal function approximation, parallel processing, and effective management of nonlinearity. The ANN model demonstrates its reliability and accuracy by achieving the highest coefficient of determination (R^2) across the training, validation, and testing subsets. The challenges for ANN include the quality and availability of data, tuning the ANN architecture for optimal performance, and requiring computational resources.

Although stress distribution along the weld path is crucial [33]–[36], most of the research has focused on predicting the SCF at the crown and saddle position. As ANN has demonstrated efficient approximation of complex phenomena [37], [38], their use in mathematical modeling SCF at a T-joint weld line is considered here. The FEA has been verified based on published results. After confirming the accuracy of the numerical model, a dataset for the Design of Experiment (DoE) was generated in ANSYS Workbench 2021 R1 [39] and was subsequently imported into MATLAB [40]. A neural network was formulated using the nntool package in MATLAB [40] with dimensionless parameters (α, β, γ, τ) as input and the SCF as output. The trained model's weights and biases were used to generate mathematical equations to calculate the SCF at the chord side of the T-joint. The SCF is computed by this model at each 15° angle about the brace axis.

2. Methodology

In ANN-based mathematical modeling, input parameter bounds are first established, and design configurations are then created, followed by finite element analysis. Finally, the weight and biases of the ANN are used to formulate the equations. Figure 2 depicts a flowchart that illustrates this methodology. The design dataset was established by describing a range of design variables frequently utilized in the offshore sector. The datasets were analyzed using FEA, and the outcomes were stored. The data was transferred to MATLAB [40] for neural network modeling. The

empirical model was developed using the ANN weights and biases from MATLAB [40]. The subsequent subsections detail these steps.

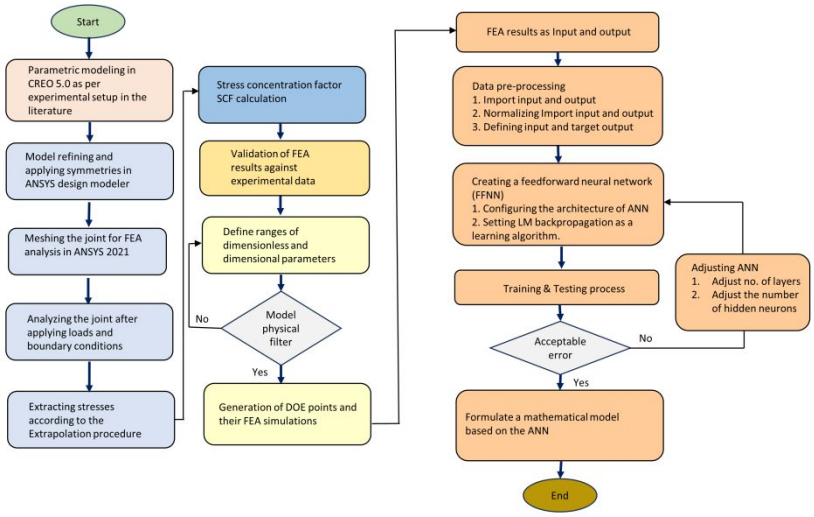

Figure 2: Methodology flowchart for ANN-based modeling of SCF.

2.1 **Finite element modeling**: Finite element modeling of T-joints with dimensionless and dimensional parameters was performed in CREO 5.0 [41] and ANSYS 2021 [39]. The models, as per the Design of Experiments (DOE), were developed in CREO 5.0 software [41] and refined in ANSYS design modeler. Linear elastic static analysis is appropriate for calculating the SCFs in tubular joints and was performed in ANSYS 2021R1 [39].

2.1.1 **Parametric modeling in CREO 5.0.** The tubular T-joint was modeled in Creo 5.0 [41]. The model, as shown in Figure 1, was built using parametric equations with dimensionless and dimensional parameters as given in Table I as variables. The parametric modeling enabled fast and efficient update of the model as per the requirement of DOE within seconds. The parts were modeled in pieces and then assembled, which helped achieve sub-zone meshing**.** Only 1/4 of the complete T-joint is modeled owing to the XY-plane and YZ-plane symmetries in the joint geometry and loading.

2.1.2 **Weld profile:** The welding profile requires careful attention for an accurate SCF. The size around the brace and chord junction is based on the AWS D 1.1 specifications (2020), and the weld profile is modeled according to AWS D 1.1 [42], as described by Lotfollahi et al. [34]. As the welded tubular connections of offshore structures are post-heated after fabrication to remove residual stresses caused by the welding process, as stated by Paradowska et al. [43], no residual stresses were considered in this study.

2.1.3 **Model refinement in Design Modeler**: The model was then imported to Design Modeler, which was used to refine the model and add symmetries and name selections.

2.1.4 **Material model:** The material parameters for the brace and chord were derived from Ragupathi et al.'s experimental coupon test findings of the steel material [44]. The steel had a yield stress of 300 MPa, an ultimate stress of 415 MPa, Young's modulus of 207.9 GPa, and a poison ratio of 0.29.

2.1.5 **Meshing:** Sub-zone meshing was adopted for the parts at the brace and chord intersection. The coarser mesh was selected for brace and chord regions which were away from the brace and chord intersections. The mesh with the number of divisions was provided to the parts around the intersection. As shown in Figure 3, the extrapolation region was meshed to obtain nodes at 15˚ around the brace and to get nodes at extrapolation points (0.4T and 1.4T Figure 4). The chord and brace were meshed separately, and ANSYS

[39] contacts were used for their connections. A sensitivity assessment led to the finalization of a mesh of 4432 elements.

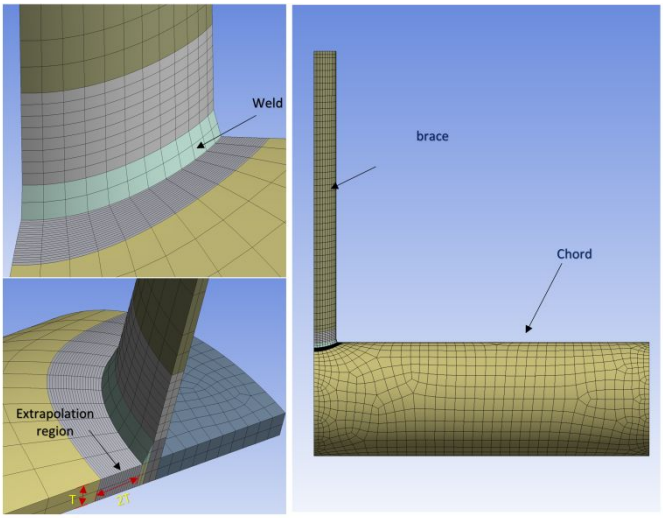

Figure 3: Mesh generated for FEA analysis of a T-joint in ANSYS 2021 [39]

2.1.6 **Boundary conditions and Loads:** The deformation was kept linearly elastic by carefully selecting the load magnitudes [45]. The end of the chord was fixed, and a pressure of 10 MPa was exerted at the top of the central brace. A pressure of 10 MPa was chosen to ensure that the stresses in the weakest joint in the Design of Experiments (DoE) remain under the elastic limit.

2.1.7 **Extraction of stresses, Extrapolation procedure and SCF calculation:** The SCFs were computed using the International Institute of Welding IIW-XVE methodology [46]. The linear extrapolation of von Mises stresses was performed at two specific locations, 0.4T and 1.4T, from the weld toe, where T denotes the chord's thickness. The studies by Ahmadi et al. [33], [47], [48] and Hosseini et al. [33], [47], [48] also utilized von Mises stress for SCF calculation. Given the complex geometry of the weld toe, the SCF zone was divided into a separate mesh. The length of the SCF zone was chosen to be twice the thickness of the chord to ensure that the node at 1.4T is not influenced by the mesh size of the chord outside the extrapolation region and to obtain nodes at a distance of 0.1T. For extrapolation points around the brace, the extrapolation region from 0˚ to 90˚ was divided into 12 equal portions to get the stresses at an angle of 15˚ from the crown position to saddle position, as shown in Figure 4. After obtaining the von Mises stresses at the fourth and fourteenth elements, the hotspot stress at the weld toe was extrapolated accordingly. The SCF was calculated by dividing the stress at the hotspot by the nominal stress of the brace.

$$SCF = {}^{\sigma_{hotspot\ stress}}\Big/_{\sigma_{nominal\ stress}} \quad \ldots\ldots\ldots\ldots\ldots (6)$$

where,

$$\sigma_{hotspot\ stress} = 1.4\sigma_1 - 0.4\sigma_2 \quad \ldots\ldots\ldots\ldots\ldots (7)$$

Where σ1 and σ2 are the stresses on the first and the second extrapolation points, respectively. The first and second extrapolation points are at 0.4*T and 1.4*T from the weld toe, respectively. The nominal stress, $\sigma_{nominal}$ can be calculated as follows.

$$\sigma_{nominal} = \frac{F}{\pi(r^2 - (r-t)^2)} \quad \ldots\ldots\ldots\ldots (8)$$

Where r and t are the radius and thickness of the brace (Figure 1), respectively.

The extrapolation points around the central brace, as recommended by the International Institute of Welding [46], are shown in Figure 4 below.

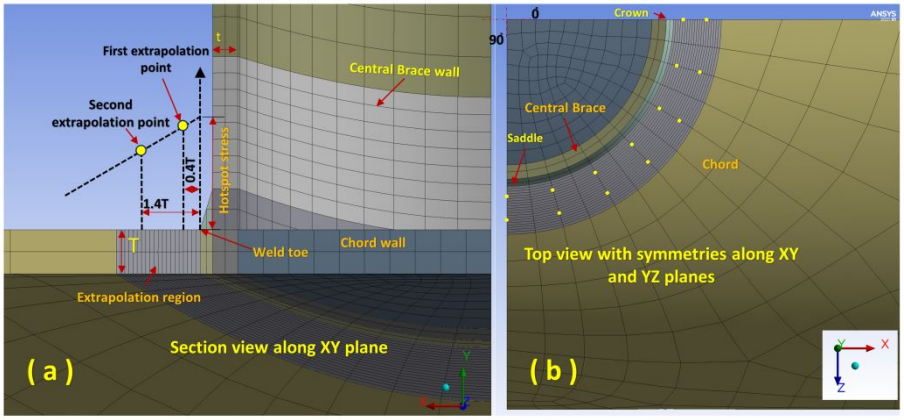

Figure 4: Extrapolation procedure as established by the International Institute of Welding IIW-XV-E-(1999) [46]

Chang et al. [22] investigated the impact of brace length on SCFs and determined that the length of the brace does not have any apparent effect on SCFs when the ratio α_b ($\alpha_b = 2\ell/d$) is greater than a crucial limit, so a length of the brace, ℓ=1000mm was selected for all simulations.

2.1.8 **Determination of the specific values for the design parameters.** The design variables serve as a function for the SCF equation. The design parameter ranges were selected from their corresponding ranges utilized in the offshore industry.

2.1.9 Development of the design dataset. The design dataset development was done in two stages. Initially, the entire range of geometric factors was taken into consideration in creating a set of design points. The dataset was then filtered based on the dimensionless parameters specified in Table I. As this dataset is large, it was reduced for further evaluation. A partial factorial design was chosen to minimize the number of simulations, incorporating five distinct values for each parameter**.**

***2.2* Utilizing the MATLAB nntool for modeling with Artificial Neural Networks (ANN).** The input data for MATLAB [40] comprised dimensionless parameters, with SCF as the output. The neural network was created by importing the data into MATLAB's nntool module [40]. ANNs rely on the universal approximation theory, which suggests that a basic neural network can estimate continuous functions depending on provided inputs [49]. The present study involved the development of an ANN method based on FEA. The objective was to establish a novel empirical formula that could accurately predict stress concentration factors of T-joints subjected to compressive loading. The Levenberg–Marquardt backpropagation algorithm was used to operationalize the concept of supervised learning. This algorithm exhibits a higher efficiency level because of its second-order convergence rate [49]–[51]. Figure 5 illustrates a typical ANN model with an input layer consisting of two inputs, a hidden layer consisting of three neurons, and an output layer with two outputs.

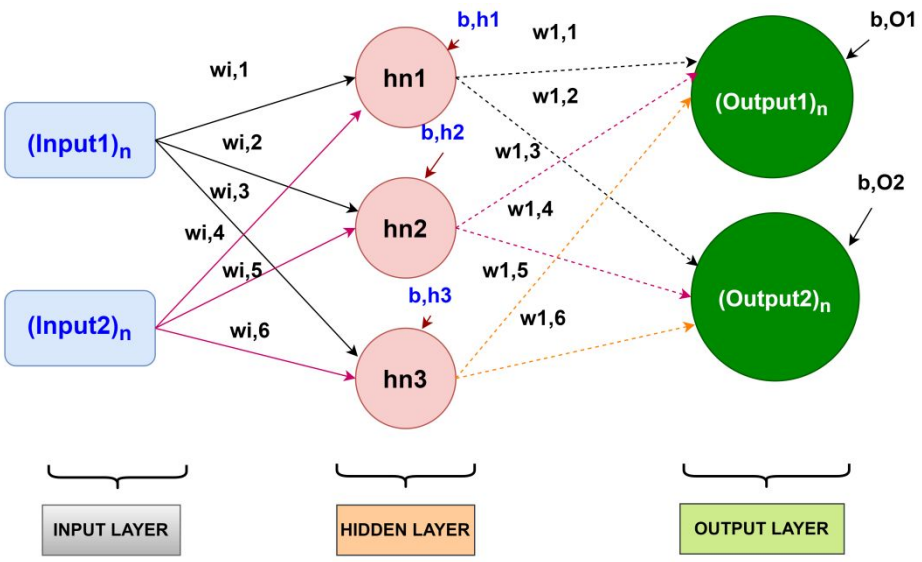

Figure 5: A typical feed-forward neural network.

The ANN underwent training using the specified input and output data. The hidden layers utilized tan-sigmoid, and the input and output layers utilized linear transfer functions, as described by Equations 9 and 10 [24], [37], [52]. The tan-sigmoid activation function exhibits a sigmoidal output like the sigmoid activation function. However, Tan-sigmoid is more preferable than sigmoid activation function as its output values are between -1 and 1, which reduces the likelihood of getting stuck [53]. Furthermore, there is no concern about activations blowing up, and its gradient is more powerful than that of the sigmoid activation function [54]. The ANN's ability to produce outcomes that closely match the training set was assessed based on the model's coefficient of determination (R^2). The R^2 value, representing the degree of correlation between the regression line of the ANN's plot and the training data points, varies from 0.0 to 1.0, with a higher R^2 value indicates a better match.

$$A(x) = \frac{2}{(1 + e^{-2x}) - 1} \quad \ldots\ldots\ldots\ldots\ldots\ldots\ldots\ldots (9)$$

$$f(x) = x \quad \ldots\ldots\ldots\ldots\ldots\ldots\ldots\ldots (10)$$

2.2.1 **Empirical modeling.** The mathematical expression representing the trained ANN weights and biases was utilized to derive the equation. Equations 11 and 12 provide the matrix form of an ANN. Every neuron in the surrounding hidden layer (hnx) is linked to the inputs (ipx) with weights (WWx). They are added after multiplying the input values by their corresponding weights. The sum of the products is combined with a bias value (Bx) and then processed through an activation function A(x). The neuron in the subsequent hidden layer takes input from the created sum until the output layer is reached.

$$\begin{bmatrix} hn1 \\ hn2 \end{bmatrix} = \begin{bmatrix} W1 & W3 & W5 \\ W2 & W4 & W6 \end{bmatrix} \begin{bmatrix} ip1 \\ ip2 \\ ip3 \end{bmatrix} + \begin{bmatrix} B1 \\ B2 \end{bmatrix} \quad \ldots\ldots\ldots\ldots\ldots\ldots\ldots\ldots (11)$$

$$[op] = \begin{bmatrix} W7 & W8 \end{bmatrix} \begin{bmatrix} hn1 \\ hn2 \end{bmatrix} + [B3] \quad \ldots\ldots\ldots\ldots\ldots\ldots\ldots\ldots (12)$$

3. Results and Discussion

Determination of the specific values for the design parameters. The geometry of the T-joint is defined by dimensionless and dimensional parameters (Figure 1). The set of dimensionless and dimensional parameters and their ranges were selected to build a dataset for the Design of Experiments (DoE) according to the established criteria in the offshore sector [8], [1], [25], [55]–[57]. Table I displays the range of these variables. A dataset consisting of 625 design points was utilized for simulation. CREO 5.0 [41] was used to do parametric modeling of the T-joint.

Table I: Parameters and their ranges.

Sr.No.	Type of parameter	Parameter	Range	References
1	Dimensionless	α	8-40	[8], [1], [25], [55]–[57]
2		β	0.3-0.7	
3		γ	12-28	
4		τ	0.4-1	
5	Dimensional	Θ	90˚	
6		D	300mm	
7		ℓ	1000mm	

Validation of FEA results against experimental data. T-joints JISSP joint 1.3 and JISSP joint 1.13 were selected from the experimental test findings documented in the HSE OTH 354 report [8] to validate the finite element analysis. The parameters associated with the geometry of the validation joints were identical to those of the experimental models and are presented in Table II. The related notations and definitions are provided in Figure 1.

Table II: Chord diameter and the other geometrical parameters of the validation joints.

Reference joint	D (mm)	α	β	γ	τ
JISSP joint 1.3 [8]	508	6.2	0.8	20.3	0.99
JISSP joint 1.13 [8]	508	6.2	0.8	20.3	1.07

The accuracy of the FEA findings was validated through a direct comparison with the experimental results reported in the JISSP1.3 and JISSP1.13 tubular T-joints [8]. Table III provides an overview of the validation at the saddle and crown. The % Error in Table III represents the percentage difference between the findings obtained from the experimental results and the finite element model. Table III shows that the finite element model accurately predicts the SCFs at the crown and saddle. This SCF prediction aligns well with the test results.

Table III: Validation of FEA results

Joint	position	Test results	Present study	% Error
JSIIP1.3	Crown	5.4	5.5	1.9
	Saddle	11.4	12.2	7.4
JSIIP1.13	Crown	4.8	4.57	4.7
	Saddle	13	10.9	16.2

Creation of the design's dataset. After the validation of the FE model, the simulations of the design dataset were conducted using CREO 5.0 [41], ANSYS [39], Python script, and MATLAB [40]. Stress values were extracted at each 15° around the brace's axis using a Python script in ANSYS Mechanical [39], and von Mises stresses at 0.4T and 1.4T were calculated. These stresses were then extrapolated to calculate the hot-spot stress at the weld toe. The linear stress extrapolation approach was used as the difference in stress between this and the nonlinear approach is less than 10%. [8]. The approach utilized by the International Institute of Welding IIW-XV-E-(1999) [46] was used to extrapolate the hot-spot stress at the weld toe. SCFs were extracted from the hot-spot values using Equation 6 and subsequently used to train the ANN. Outputs were successfully generated for 625 design configurations. For every iteration, six output parameters were defined, specifically SCF at every 15° offset (for a total of 90°) due to symmetries in XY and YZ planes.

Response of dimensionless parameters on SCF. All dimensionless parameters (α, β, γ, and τ) have a significant effect on HSS and SCF. The definitions of these parameters are provided in Figure 1. Increasing the value of α increases the length of the chord at a constant chord diameter, leading to higher HSS and SCF due to increased strain resulting from the increased length at a constant chord diameter. By increasing the value of β, the diameter of the brace increases at a constant chord diameter. The effect of β on HSS and SCF is parabolic. Increasing the value of β from 0.3 to 0.5 results in an increase in HSS and SCF, while increasing β from 0.5 to 0.7 results in a decrease in HSS and SCF. This is due to the change of load from punching shear at low β to local bending and ovalization at higher β [58]. Higher values of γ at a constant chord diameter result in a thinner chord, which leads to higher HSS and SCF [59]. A higher value of τ at a constant chord thickness results in a thicker brace, increasing the HSS and SCF [60].

Utilizing the MATLAB nntool for modeling with ANN. The ANN was trained using a dataset consisting of 625 simulated design points. An ANN model was established using dimensionless parameters (α, β, ɣ, τ) as input and the SCF at a 15° offset as output. A feed-forward neural network (FFNN) design, which has an input layer, a hidden layer (or layers), and an output layer, was used. Figure 6 displays the architecture of the developed ANN model.

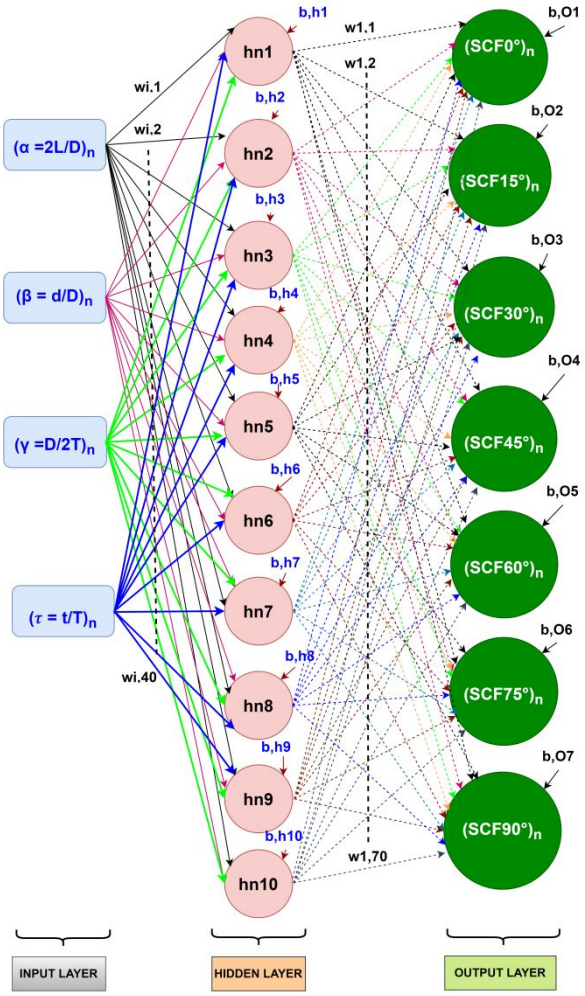

Figure 6: The developed ANN.

The optimal configuration of the neural network was determined by iteratively adjusting the total number of hidden layers and the hidden neurons through the trial and error method [37]. An ANN was constructed with one input layer, one hidden layer and an output layer. The hidden layer contains ten neurons. The training set received 70% of the whole design dataset, while 15% was allocated for both validation and testing during the training process.

The ANN exhibited a high level of accuracy, with an R^2 value of 0.998. The predictions by the ANN were strongly correlated with the SCFs of a T-joint under compressive load, as determined by FEA.

Figure 7 depicts the regression plots produced by MATLAB R2021 [40] for the ANN. The diagram consists of four plots, each representing the training, validation, testing, and three plots combined. The graphs display the linear regression line of best fit, which represents the relationship between the output of the ANN and the desired output value. The solid lines reflect this line of best fit, while the dashed lines show the ideal or perfect outcomes. Figure 7 demonstrates that the solid lines and dotted lines in each plot exhibit a nearly perfect overlap, suggesting that the ANN can produce outputs that closely resemble the training data. Under training, validation, and testing subsets, a minimum R^2 value of 0.996 is achieved, demonstrating the consistency and reliability of the suggested ANN model.

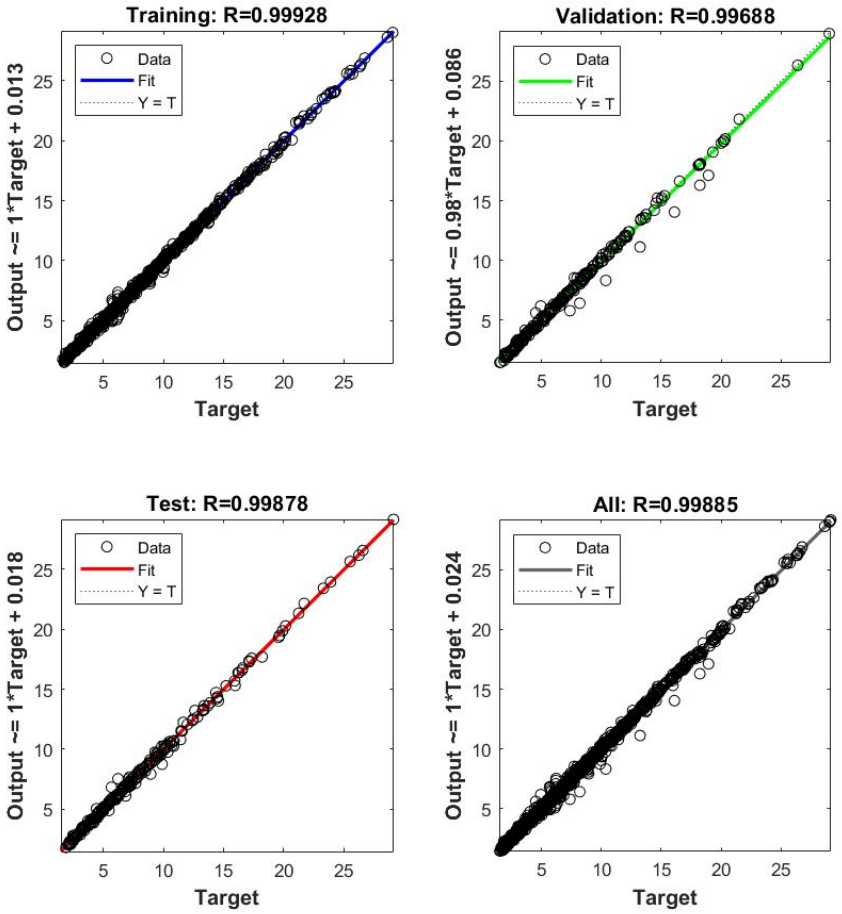

Figure 7: Trained ANN Regression plots.

The performance graphs of the trained ANN throughout the validation procedure are shown in Figure 8. The best epoch yielded the weights for each neuron and biases for each layer, which were used for empirical modeling.

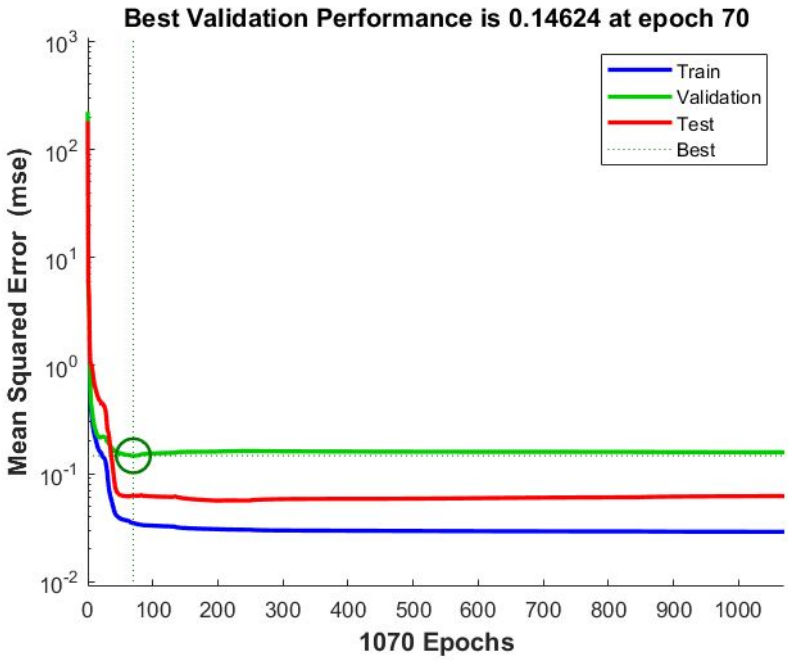

Figure 8: Performance validation of trained ANN.

Empirical modeling. The ANN's weights and biases were exported as a matrix. Prior to being used in numerical equations for standardization, it is necessary to normalize the inputs to prevent particular variables from dominating the result. The outputs must be denormalized afterwards. Normalization and denormalization can be performed using Equations 13 and 14, while the derived empirical formulas for SCF are given in Equations 15 and 16.

$$i_{normalized} = i_{n,min} + \frac{(i_{n,max} - i_{n,min})(i - i_{min})}{(i_{max} - i_{min})} \quad \text{..... Equation 13}$$

$$o_{denormalized} = o_{min} + \frac{(o_n - o_{n,min})(o_{max} - o_{min})}{(o_{n,max} - o_{n,min})} \quad \text{..... Equation 14}$$

where, $i_{n,max} = 1$ i_{max} = maximum of original input data

$i_{n,min} = -1$ i_{min} = minimum of original input data

$o_{n,max} = 1$ o_{max} = maximum of SCF data used for training

$o_{n,min} = -1$ o_{min} = minimum of SCF data used for training

$$\begin{bmatrix} h1 \\ h2 \\ h3 \\ h4 \\ h5 \\ h6 \\ h7 \\ h8 \\ h9 \\ h10 \end{bmatrix} = \begin{bmatrix} -0.05 & 0.27 & -0.39 & 0.87 \\ 0.03 & -0.34 & -0.56 & -0.04 \\ 0 & 0.52 & 0.20 & -0.27 \\ 0.06 & -0.71 & 0.05 & 0.20 \\ -1.50 & 0.14 & 0.25 & 0.33 \\ 0.46 & 0.34 & -0.08 & 0.33 \\ -0.04 & 0.17 & -0.50 & -1.49 \\ -1.76 & 0.12 & 0.34 & 0.25 \\ 0.08 & -0.61 & -0.93 & 0.06 \\ -0.02 & 0.38 & 0.36 & 0 \end{bmatrix} \begin{bmatrix} \alpha n \\ \beta n \\ \gamma n \\ \tau n \end{bmatrix} + \begin{bmatrix} 1.25 \\ -0.02 \\ 0.59 \\ 0.05 \\ -1.85 \\ -1.35 \\ 1.54 \\ -2.58 \\ -0.12 \\ -0.70 \end{bmatrix} \quad \text{..... Equation 15}$$

$$\begin{bmatrix} SCF\ 0^\circ \\ SCF\ 15 \\ SCF\ 30 \\ SCF\ 45 \\ SCF\ 60 \\ SCF\ 75 \\ SCF\ 90 \end{bmatrix} = \begin{bmatrix} 0.23 & -1.30 & -0.56 & -0.02 & -0.85 & 1.95 & 0.01 & 1.54 & 0.59 & -0.42 \\ 0.28 & -1.47 & -0.48 & 0.06 & -0.72 & 1.93 & -0.03 & 1.26 & 0.61 & -0.60 \\ 0.41 & -2.30 & -0.40 & 0.14 & -0.53 & 1.69 & -0.12 & 0.75 & 0.81 & -1.37 \\ 0.52 & -2.39 & -0.01 & 0.35 & -0.12 & 0.85 & -0.22 & -0.16 & 0.76 & -1.54 \\ 0.65 & -1.69 & 0.60 & 0.75 & 0.35 & 0.29 & -0.32 & -1.10 & 0.48 & -0.76 \\ 0.71 & -0.91 & 0.99 & 1.05 & 0.61 & -0.03 & -0.38 & -1.60 & 0.27 & 0.24 \\ 0.73 & -0.63 & 1.14 & 1.16 & 0.66 & -0.15 & -0.40 & -1.71 & 0.22 & 0.67 \end{bmatrix} \begin{bmatrix} h1 \\ h2 \\ h3 \\ h4 \\ h5 \\ h6 \\ h7 \\ h8 \\ h9 \\ h10 \end{bmatrix} + \begin{bmatrix} 1.82 \\ 1.53 \\ 0.68 \\ -0.83 \\ -1.70 \\ -1.90 \\ -1.90 \end{bmatrix} \quad \text{.....Equation 16}$$

A dataset that was not part of the training, validation, or test data set was used to validate the empirical model. Table IV displays six validation design points together with their respective maximum absolute and percentage differences. Figure 9 displays a comparison between the SCF calculated using FEA in ANSYS Workbench [39] and ANN from the proposed empirical model.

$$\text{Error (\%)} = \left(\frac{(Predicted\ value - FEA\ value)}{FEA\ value}\right) * 100 \quad \text{.....Equation 17}$$

Table IV: Empirical model verification results

Sr. No	α	β	γ	τ	Max. absolute difference	Maximum % Error

1	15	0.28	16.3	0.65	0.17	4.8
2	31	0.29	15.9	0.75	0.48	-5.1
3	31.8	0.52	15.4	0.43	0.26	4.9
4	23.7	0.47	16.3	0.35	0.23	-4.9
5	8.5	0.63	27.3	0.95	0.96	-5.2
6	10	0.75	26	0.79	0.50	-5.4

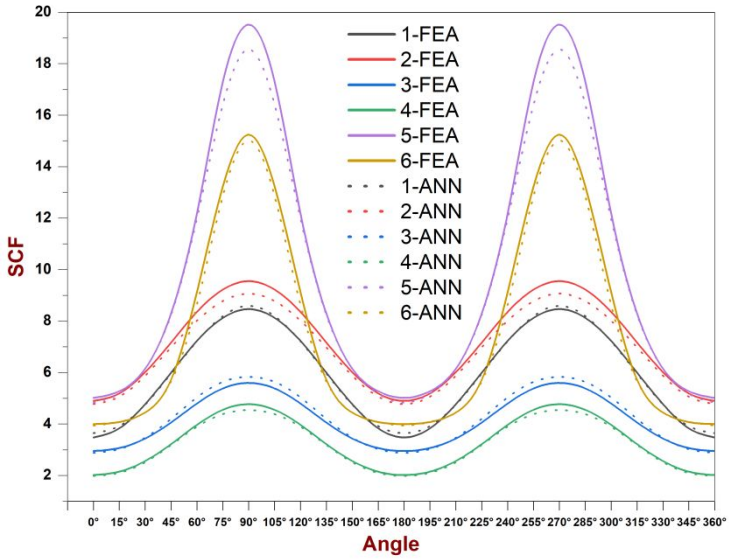

Figure 9: Outcomes of ANN and FEA.

In a brief period, the derived equations precisely calculate the SCF, with a discrepancy of less than 6% percentage error (Equation 17) compared to the SCF computed by FEA. Therefore, these equations can be used to compute the SCF along the axis of the brace in a T-joint under axial compressive load.

CONCLUSIONS

The equations developed using ANN are an efficient approach for determining the SCF in tubular joints. The integration of FEA with ANN has proven to be successful in estimating SCF. The provided equations can forecast the SCF around the weld toe of the T-joint with a percentage error of under 6% for designated angles. These remain valid even if the maximum SCF position differs from the saddle or crown position. Engineers in practice can use the equations (Equation 13-14) to compute the hotspot stress precisely and rapidly, thereby minimizing risks linked to fatigue failure of offshore structures and assuring their longevity and reliability. Our research contributes to enhancing the safety and reliability of offshore structures by facilitating more precise assessments of stress distribution.

The dimensionless parameters have a significant impact on HSS and SCF. Increasing the parameters (α, γ and τ) increase the HSS and SCF while increasing the parameter β has a parabolic effect. Increasing β from 0.3 to 0.5 increases the HSS and SCF, while increasing the β from 0.5 to 0.7 decreases HSS and SCF.

SCF of tubular joints with inclined braces can also be calculated using an identical approach. Likewise, the same procedure can be used for the T-joint subjected to IPB, OPB, or mixed-stress situations. This approach can be applied to different types of joints to derive a set of equations that can be used for efficient computations of the SCF. The estimation of SCF (Stress Concentration Factor) can be improved by considering the parameters associated with the defects.

Funding

This research received funding from Yayasan Universiti Teknologi PETRONAS under grant No. 015LC0-443.

REFERENCES

[1] H. Ahmadi, M. Ali Lotfollahi-Yaghin, S. Yong-Bo, and M. H. Aminfar, "Parametric study and formulation of outer-brace geometric stress concentration factors in internally ring-stiffened tubular KT-joints of offshore structures," *Appl. Ocean Res.*, vol. 38, pp. 74–91, 2012, doi: 10.1016/j.apor.2012.07.004.

[2] H. Ahmadi, M. A. Lotfollahi-Yaghin, and M. H. Aminfar, "Effect of stress concentration factors on the structural integrity assessment of multi-planar offshore tubular DKT-joints based on the fracture mechanics fatigue reliability approach," *Ocean Eng.*, vol. 38, no. 17–18, pp. 1883–1893, 2011, doi: 10.1016/j.oceaneng.2011.08.004.

[3] X. Xu, Y. Shao, X. Gao, and H. S. Mohamed, "Stress concentration factor (SCF) of CHS gap TT-joints reinforced with CFRP," *Ocean Eng.*, vol. 247, no. January, p. 110722, 2022, doi: 10.1016/j.oceaneng.2022.110722.

[4] S. Petinov and R. Guchinsky, "Criteria for Fatigue Failure of Materials: Application in Fatigue Assessment of Structures," *Adv. Eng. Forum*, vol. 26, pp. 1–8, 2018, doi: 10.4028/www.scientific.net/aef.26.1.

[5] J. Wardenier, Y. Kurobane, J. A. Packer, G. J. Van der Vegte, and X.-L. Zhao, *Design guide for circular hollow section (CHS) joints under predominantly static loading*. Cidect, 2008.

[6] P. Smedley and P. Fisher, "Stress concentration factors for simple tubular joints," in *ISOPE International Ocean and Polar Engineering Conference*, 1991, p. ISOPE-I.

[7] A. K. Hellier, M. P. Connolly, and W. D. Dover, "Stress concentration factors for tubular Y- and T-joints," *Int. J. Fatigue*, vol. 12, no. 1, pp. 13–23, 1990, doi: 10.1016/0142-1123(90)90338-F.

[8] U. K. HSE, "OTH 354 (1997) Stress Concentration Factors for Simple Tubular Joints-Assessment of Existing and Development of New Parametric Formulae," *Prep. by Lloyd's Regist. Shipp. UK*.

[9] J. G. Kuang, A. B. Potvin, and R. D. Leick, "Stress Concentration in Tubular Joints," *Offshore Technology Conference*. p. OTC-2205-MS, May 04, 1975. doi: 10.4043/2205-MS.

[10] A. C. Wordsworth and G. P. Smedley, "Stress concentrations at unstiffened tubular joints," in *European Offshore Steels Research Seminar[Proc. Conf.]*, 1978.

[11] U. E. G. (UEG), "Design of tubular joints for offshore structures," *UEG Publ.*, vol. 2, pp. 43–60, 1985.

[12] Mjrd. Efthymiou, "Development of SCF formulae and generalised influence functions for use in fatigue analysis." OTJ, 1988.

[13] H. Nassiraei and P. Rezadoost, "Stress concentration factors in tubular T/Y-joints strengthened with FRP subjected to compressive load in offshore structures," *Int. J. Fatigue*, vol. 140, no. June, p. 105719, 2020, doi: 10.1016/j.ijfatigue.2020.105719.

[14] K. Roy, H. Rezaeian, D. Lakshmanan, Z. Fang, G. Beulah Gnana Ananthi, and J. B. P. Lim, "Structural behaviour of cold-formed steel T-Stub connections with HRC and screws subjected to tension force," *Eng. Struct.*, vol. 283, no. February, p. 115922, 2023, doi: 10.1016/j.engstruct.2023.115922.

[15] D. L. Chandramohan, K. Roy, H. Taheri, M. Karpenko, Z. Fang, and J. B. P. Lim, "A State of the Art Review of Fillet Welded Joints," *Materials (Basel).*, vol. 15, no. 24, pp. 1–31, 2022, doi: 10.3390/ma15248743.

[16] R. Feng, C. Tang, K. Roy, Z. Chen, B. Chen, and J. B. P. Lim, "An experimental study on stress concentration factors of stainless steel hybrid tubular K-joints," *Thin-Walled Struct.*, vol. 157, no. September, p. 107064, 2020, doi: 10.1016/j.tws.2020.107064.

[17] R. Feng, L. Chen, Z. Chen, B. Chen, K. Roy, and J. B. P. Lim, "Experiments on stainless steel hybrid K-joints with square braces and circular chord," *J. Constr. Steel Res.*, vol. 185, no. August, p. 106865, 2021, doi:

10.1016/j.jcsr.2021.106865.

[18] R. Feng, C. Tang, Z. Chen, K. Roy, B. Chen, and J. B. P. Lim, "A numerical study and proposed design rules for stress concentration factors of stainless steel hybrid tubular K-joints," *Eng. Struct.*, vol. 233, no. June 2020, p. 111916, 2021, doi: 10.1016/j.engstruct.2021.111916.

[19] R. Feng, J. Xu, Z. Chen, K. Roy, B. Chen, and J. B. P. Lim, "Numerical investigation and design rules for stress concentration factors of stainless-steel hybrid tubular joints," *Thin-Walled Struct.*, vol. 163, no. April, p. 107783, 2021, doi: 10.1016/j.tws.2021.107783.

[20] D. S. Saini, D. Karmakar, and S. Ray-Chaudhuri, "A review of stress concentration factors in tubular and non-tubular joints for design of offshore installations," *J. Ocean Eng. Sci.*, vol. 1, no. 3, pp. 186–202, 2016, doi: 10.1016/j.joes.2016.06.006.

[21] H. Nassiraei, M. A. Lotfollahi-Yaghin, and H. Ahmadi, "Static strength of offshore tubular T/Y-joints reinforced with collar plate subjected to tensile brace loading," *Thin-Walled Struct.*, vol. 103, pp. 141–156, 2016, doi: 10.1016/j.tws.2016.02.010.

[22] E. Chang and W. D. Dover, "Parametric equations to predict stress distributions along the intersection of tubular X and DT-joints," *Int. J. Fatigue*, vol. 21, no. 6, pp. 619–635, 1999, doi: 10.1016/S0142-1123(99)00018-3.

[23] K. C. Gulati, W. J. Wang, and D. K. Y. Kan, "An Analytical Study of Stress Concentration Effects in Multibrace Joints Under Combined Loading," *Offshore Technology Conference*. p. OTC-4407-MS, May 03, 1982. doi: 10.4043/4407-MS.

[24] M. Iqbal, S. Karuppanan, B. S. Iskandar, and V. Perumal, "analysis and artificial neural networks for the fatigue design of tubular KT- Empirical modeling of stress concentration factors using finite element analysis and artificial neural networks for the fatigue design of tubular KT-joints under combined loadin," no. August, 2023, doi: 10.1111/ffe.14122.

[25] H. Ahmadi and E. Zavvar, "Stress concentration factors induced by out-of-plane bending loads in ring-stiffened tubular KT-joints of jacket structures," *Thin-Walled Struct.*, vol. 91, pp. 82–95, 2015, doi: 10.1016/j.tws.2015.02.011.

[26] N. ISO 19902, "Petroleum and natural gas industries—Fixed steel offshore structures," *Int. Organ. Stand.*, 2007.

[27] G. L. Dnv, "DNVGL-RP-C203: Fatigue design of offshore steel structures," *DNV GL, Oslo, Norw.*, 2016.

[28] A. P. I. RP2A-WSD, "Recommended practice for planning, designing and constructing fixed offshore platforms–working stress design–," *Twenty-2000*, 2000.

[29] S. Wang *et al.*, "Automatic laser profile recognition and fast tracking for structured light measurement using deep learning and template matching," *Meas. J. Int. Meas. Confed.*, vol. 169, no. May 2020, 2021, doi: 10.1016/j.measurement.2020.108362.

[30] V. T. Tran, T. K. Nguyen, H. Nguyen-Xuan, and M. Abdel Wahab, "Vibration and buckling optimization of functionally graded porous microplates using BCMO-ANN algorithm," *Thin-Walled Struct.*, vol. 182, no. November 2022, 2023, doi: 10.1016/j.tws.2022.110267.

[31] T. Nghia-Nguyen, M. Kikumoto, H. Nguyen-Xuan, S. Khatir, M. Abdel Wahab, and T. Cuong-Le, "Optimization of artificial neutral networks architecture for predicting compression parameters using piezocone penetration test," *Expert Syst. Appl.*, vol. 223, no. March, 2023, doi: 10.1016/j.eswa.2023.119832.

[32] B. L. Dang, H. Nguyen-Xuan, and M. Abdel Wahab, "An effective approach for VARANS-VOF modelling interactions of wave and perforated breakwater using gradient boosting decision tree algorithm," *Ocean Eng.*, vol. 268, no. November 2022, 2023, doi: 10.1016/j.oceaneng.2022.113398.

[33] H. Ahmadi, M. A. Lotfollahi-Yaghin, and M. H. Aminfar, "Geometrical effect on SCF distribution in uni-planar tubular DKT-joints under axial loads," *J. Constr. Steel Res.*, vol. 67, no. 8, pp. 1282–1291, 2011, doi: 10.1016/j.jcsr.2011.03.011.

[34] M. A. Lotfollahi-Yaghin and H. Ahmadi, "Effect of geometrical parameters on SCF distribution along the weld toe of tubular KT-joints under balanced axial loads," *Int. J. Fatigue*, vol. 32, no. 4, pp. 703–719, 2010, doi: 10.1016/j.ijfatigue.2009.10.008.

[35] E. Chang and W. D. Dover, "Stress concentration factor parametric equations for tubular X and DT joints," *Int. J. Fatigue*, vol. 18, no. 6, pp. 363–387, 1996, doi: 10.1016/0142-1123(96)00017-5.

[36] A. N'Diaye, S. Hariri, G. Pluvinage, and Z. Azari, "Stress concentration factor analysis for welded, notched tubular T-joints under combined axial, bending and dynamic loading," *Int. J. Fatigue*, vol. 31, no. 2, pp. 367–374, 2009, doi: 10.1016/j.ijfatigue.2008.07.014.

[37] M. Lo, S. Karuppanan, and M. Ovinis, "ANN-and FEA-Based Assessment Equation for a Corroded Pipeline with a Single Corrosion Defect," *J. Mar. Sci. Eng.*, vol. 10, no. 4, 2022, doi: 10.3390/jmse10040476.

[38] K. Miao, Z. Pan, A. Chen, Y. Wei, and Y. Zhang, "Machine learning-based model for the ultimate strength of circular concrete-filled fiber-reinforced polymer–steel composite tube columns," *Constr. Build. Mater.*, vol. 394, no. May, p. 132134, 2023, doi: 10.1016/j.conbuildmat.2023.132134.

[39] "Ansys Workbench | Simulation Integration Platform." [Online]. Available: https://www.ansys.com/products/ansys-workbench

[40] "R2021a - Updates to the MATLAB and Simulink product families - MATLAB & Simulink." [Online]. Available: https://www.mathworks.com/products/new_products/release2021a.html

[41] "Creo CAD Software: Enable the Latest in Design | PTC." [Online]. Available: https://www.ptc.com/en/products/creo

[42] American National Standard Structural Welding, *Aws D1 .1/D1 .1 M:2020*. 2020.

[43] A. Paradowska, J. Price, P. Dayawansa, B. Kerezsi, X.-L. Zhao, and R. Ibrahim, "Study of influence of post weld heat treatment on residual stress distribution in tubular joints," *Weld. Res. Abroad*, vol. 52, pp. 10–19, Jan. 2006.

[44] R. Masilamani and S. Nallayarasu, "Experimental and numerical investigation of ultimate strength of ring-stiffened tubular T-joints under axial compression," *Appl. Ocean Res.*, vol. 109, no. February, p. 102576, 2021, doi: 10.1016/j.apor.2021.102576.

[45] H. Ahmadi, M. A. Lotfollahi-Yaghin, and S. Yong-Bo, "Chord-side SCF distribution of central brace in internally ring-stiffened tubular KT-joints: A geometrically parametric study," *Thin-Walled Struct.*, vol. 70, pp. 93–105, 2013, doi: 10.1016/j.tws.2013.04.011.

[46] IIW-XV-E, "Recommended fatigue design procedure for welded hollow section joints." International Institute of Welding France, 1999.

[47] A. S. Hosseini, M. R. Bahaari, and M. Lesani, "SCF distribution in FRP-strengthened tubular T-joints under brace axial loading," *Sci. Iran.*, vol. 27, no. 3 A, pp. 1113–1129, 2020, doi: 10.24200/SCI.2018.5471.1293.

[48] A. Sadat Hosseini, M. R. Bahaari, and M. Lesani, "Stress concentration factors in FRP-strengthened offshore steel tubular T-joints under various brace loadings," *Structures*, vol. 20, no. July, pp. 779–793, 2019, doi: 10.1016/j.istruc.2019.07.004.

[49] S. Koric, A. Viswantah, D. W. Abueidda, N. A. Sobh, and K. Khan, "Deep learning operator network for plastic deformation with variable loads and material properties," *Eng. Comput.*, no. 0123456789, 2023, doi: 10.1007/s00366-023-01822-x.

[50] S. D. V. Kumar, S. Karuppanan, and M. Ovinis, "Failure pressure prediction of high toughness pipeline with a single corrosion defect subjected to combined loadings using artificial neural network (Ann)," *Metals (Basel).*, vol. 11, no. 2, pp. 1–25, 2021, doi: 10.3390/met11020373.

[51] F. S. Panchal and M. Panchal, "Review on Methods of Selecting Number of Hidden Nodes in Artificial Neural Network," *Int. J. Comput. Sci. Mob. Comput.*, vol. 3, no. 11, pp. 455–464, 2014, [Online]. Available: www.ijcsmc.com

[52] K. Subjected, A. Compressive, M. Iqbal, S. Karuppanan, and V. Perumal, "An Artificial Neural Network Model for the Stress Concentration Factors in An Artificial Neural Network Model for the Stress Concentration Factors in KT-Joints Subjected to Axial Compressive Load," no. October, 2023, doi: 10.4028/p-YpO50i.

[53] O. A. Montesinos López, A. Montesinos López, and J. Crossa, "Fundamentals of Artificial Neural Networks and Deep Learning BT - Multivariate Statistical Machine Learning Methods for Genomic Prediction," O. A. Montesinos López, A. Montesinos López, and J. Crossa, Eds. Cham: Springer International Publishing, 2022, pp. 379–425. doi: 10.1007/978-3-030-89010-0_10.

[54] J. Feng and S. Lu, "Performance Analysis of Various Activation Functions in Artificial Neural Networks," *J. Phys. Conf. Ser.*, vol. 1237, no. 2, 2019, doi: 10.1088/1742-6596/1237/2/022030.

[55] H. Ahmadi and M. A. Lotfollahi-Yaghin, "Stress concentration due to in-plane bending (IPB) loads in ring-stiffened tubular KT-joints of offshore structures: Parametric study and design formulation," *Appl. Ocean Res.*, vol. 51, pp. 54–66, 2015, doi: 10.1016/j.apor.2015.02.009.

[56] H. Ahmadi, A. Yeganeh, A. H. Mohammadi, and E. Zavvar, "Probabilistic analysis of stress concentration factors in tubular KT-joints reinforced with internal ring stiffeners under in-plane bending loads," *Thin-Walled Struct.*, vol. 99, pp. 58–75, 2016, doi: 10.1016/j.tws.2015.11.010.

[57] H. Ahmadi and M. A. Lotfollahi-yaghin, "Experimental and Numerical Investigation of Geometric SCFs in Internally Ring-Stiffened Tubular KT-Joints of Offshore Structures," *J. Persian Gulf*, vol. 43, no. 1, pp. 7–8, 2013, [Online]. Available: http://jpg.inio.ac.ir/files/site1/user_files_c8faec/admin-A-10-1-79-4c653d4.pdf

[58] G. C. S. Krishna and S. Nallayarasu, "Experimental and numerical investigation on stress concentration at brace-ring intersection (BRI) of internally ring stiffened tubular T-joints," *Appl. Ocean Res.*, vol. 126, no. April, p. 103288, 2022, doi: 10.1016/j.apor.2022.103288.

[59] A. Sadat Hosseini, E. Zavvar, and H. Ahmadi, "Stress concentration factors in FRP-strengthened steel tubular KT-joints," *Appl. Ocean Res.*, vol. 108, no. September 2020, p. 102525, 2021, doi: 10.1016/j.apor.2021.102525.

[60] S. Bao, W. Wang, Y. H. Chai, and X. Li, "Hot spot stress parametric equations for three-planar tubular Y-joints subject to in-plane bending moment," *Thin-Walled Struct.*, vol. 149, no. August 2019, p. 106648, 2020, doi: 10.1016/j.tws.2020.106648.